Available online at www.sciencedirect.com

SCIENCE DIRECT®

International Journal of Heat and Mass Transfer 49 (2006) 3895–3905

International Journal of HEAT and MASS TRANSFER

www.elsevier.com/locate/ijhmt

# Heat transfer model for small-scale air-cooled spark-ignition four-stroke engines

Yuh-Yih Wu *, Bo-Chiuan Chen, Feng-Chi Hsieh

*Department of Vehicle Engineering, National Taipei University of Technology, 1, Sec. 3, Chung-Hsiao E. Road, Taipei 106, Taiwan, ROC*

Received 18 January 2006; received in revised form 1 March 2006
Available online 27 June 2006

**Abstract**

The heat transfer models proposed in previous studies are not suitable for small-scale spark-ignition engines, because they were developed primarily for large-scale engines. In order to improve the accuracy of the predicted heat transfer rate for small-scale engines, a heat transfer model using the Stanton number is proposed in this paper. Prediction results of instantaneous heat flux, global engine heat transfer, and cylinder pressure based on the proposed model are compared with the experimental results and prediction results of previous models. It is found that the proposed model has prediction results closer to the measured data than the previous models at most engine operating conditions.


*Keywords:* Engine heat transfer model; Stanton number; Spark-ignition engine; Heat flux

## 1. Introduction

The heat transfer model can be used to predict the engine heat transfer rate, which is very important for thermal load analysis, combustion performance prediction, and cycle simulation. Most investigations of heat transfer in spark-ignition (SI) engines are large-scale ones. Oguri [1] used Eichelberg's model to predict the heat transfer rate of a 1400 $cm^3$ SI engine, yielding predicted results that agreed with the experimental results for the expansion stroke, but not for the compression stroke. This might be because the model was established for diesel engines and was not suitable for SI engines. Alkidas [2,3] measured the instantaneous heat flux on the cylinder head of an 820 $cm^3$ four-stroke SI engine and found that it could be affected by the engine speed, air–fuel ratio, and volumetric efficiency. Alkidas and Suh [4] investigated the effects of swirl or tumble motion on the heat transfer and combustion characteristics of a single-cylinder four-valve 400 $cm^3$ SI engine. It was found that increasing swirl or tumble motions might raise the peak rate of heat release, the local surface temperature, and heat flux, on the cylinder head. Shayler [5] utilized two methods to obtain the instantaneous heat flux of the combustion chamber. In the first method, the first law of thermodynamics was applied to calculate the heat transfer rate, but the results were not accurate due to uncertain gas properties. In the second method, the heat transfer rates were calculated based on Woschni's, Annand's, and Eichelberg's experimental models. It was found that Eichelberg's model could produce prediction results closest to the experimental data.

Previous studies have focused on developing heat transfer models for large-scale engines. However, the heat transfer characteristics of large-scale and small-scale engines are quite different. For large-scale SI engines, about one-third of the fuel energy is transformed to heat loss from the cylinder body. But for a small-scale 125 $cm^3$ two-stroke SI engine, Franco [6] found that approximately 50% of the fuel energy is converted to heat loss, which is much higher than that of large-scale SI engines. Since the heat transfer

* Corresponding author. Tel.: +886 2 27712171 3620; fax: 886 2 27314990.
*E-mail address:* cyywu@ntut.edu.tw (Y.-Y. Wu).

0017-9310/$ - see front matter © 2006 Elsevier Ltd. All rights reserved.
doi:10.1016/j.ijheatmasstransfer.2006.03.043

**Nomenclature**

*Notation*

| | |
|---|---|
| $A$ | area of the heat absorbing surface ($m^2$) |
| $A_n$, $B_n$ | Fourier coefficients (dimensionless) |
| $B$ | bore diameter (m) |
| $C_m$ | mean piston speed m/s |
| $c$ | specific heat (J/kg K) |
| EOC | end of combustion (deg) |
| $h$ | heat transfer coefficient ($W/m^2$ K) |
| $k$ | thermal conductivity (W/m K) |
| $m$ | mass (kg) |
| MFB | mass fraction burned (%) |
| $N$ | total harmonic number (dimensionless) |
| $n$ | harmonic number (dimensionless) |
| $P$ | pressure ($N/m^2$) |
| $Q$ | heat (J) |
| $R$ | gas constant (kJ/kg K) |
| $Re$ | Reynolds number (dimensionless) |
| SOC | start of combustion (deg) |
| $St$ | Stanton number (dimensionless) |
| $T$ | temperature (K) |
| $t$ | time (s) |
| $u$ | turbulent fluctuating velocity (m/s) |
| $V$ | volume ($m^3$) |
| $x$ | distance (m) |
| $\alpha$ | thermal diffusivity ($m^2$/s) |
| $\gamma$ | the ratio of specific heats (dimensionless) |
| $\varepsilon$ | emissivity (dimensionless) |
| $\eta_v$ | volumetric efficiency (dimensionless) |
| $\theta$ | crank angle (deg) |
| $\theta_0$ | start of combustion timing (deg) |
| $\theta_d$ | total combustion duration (deg) |
| $\mu$ | dynamic viscosity (kg/m s) |
| $\rho$ | density ($kg/m^3$) |
| $\tau$ | time period of the temperature (s) |
| $\omega$ | angular speed (rad/s) |

*Subscripts*

| | |
|---|---|
| ai | airflow into the intake manifold |
| ao | airflow out of the intake manifold |
| conv | convective |
| cyl | cylinder |
| cc | combustion chamber |
| d | displacement |
| e | engine |
| f | fuel |
| g | gas |
| HV | heating value |
| ht | heat transfer |
| hr | heat release |
| im | intake manifold |
| m | mean value |
| p | piston or constant pressure |
| r | radiant |
| sp | spark plug |
| w | wall |

characteristics of small-scale engine are different from that of large-scale engine, it is important to develop a heat transfer model specific for four-stroke small-scale SI engines.

This paper studies the heat transfer characteristic of a 125 $cm^3$ air-cooled four-stroke SI engine, and develops a corresponding heat transfer model. The remainder of this paper is organized as follows. Section 2 introduces previous heat transfer models. The heat flux obtained from the measured temperatures is then used to establish the heat transfer model in Section 3. The heat transfer model is used for engine simulation and the engine model is described in Section 4. Simulation results of cylinder pressure are compared with the experimental results in Section 5. Finally, conclusions are made in Section 6.

## 2. Modeling of the heat transfer coefficient

The heat transfer rate $Q_{ht}$ from the flowing gas to the combustion chamber wall is dominated by the forced convection [7,8] and can be expressed as

$$\frac{\mathrm{d}hQ_{ht}}{\mathrm{d}t} = h \cdot A \cdot (T_g - T_w) \tag{1}$$

where $A$ is the area of the heat transfer surface, which is often defined as the entire surface of the combustion chamber [3,7,10,17]; $h$ is the empirical heat transfer coefficients, which is assumed the same for the entire heat transfer surface; $T_w$ is the measured temperature of the inside wall surface of the combustion chamber; and $T_g$ is the temperature of the flowing gas, which can be obtained using the state equation of ideal gas [1,9–13] as follows:

$$T_g = \frac{P_{cyl} \cdot V_{cyl}}{m_a \cdot R} \tag{2}$$

where $P_{cyl}$ is the cylinder gas pressure, $V_{cyl}$ is the cylinder volume, $m_a$ is the air mass in the cylinder, and $R$ is the gas constant.

Many models have been proposed for the heat transfer coefficient $h$ assuming that the heat flux is the same for the entire heat transfer surface. Several previous models and the proposed model will be applied to obtain the curve fitted heat transfer coefficient $h$ for the target engine.

### 2.1. Previous models

Nusselt's model was the first engine heat transfer model based on a spherical bomb, originally it was used to predict the steady-state heat flux. It can also be used to predict the instantaneous heat flux, if it is expressed in terms of instantaneous $P_{cyl}$ and $T_g$ [15,16] as

$$h = h_c + h_r \tag{3}$$

where $h_c$ and $h_r$ are the heat transfer coefficients for convection and radiation, respectively, and can be expressed as

$$h_c = a \cdot (1 + 1.24C_m) \cdot (P_{cyl}^2 \cdot T_g)^{\frac{1}{3}}, \quad \text{unit} = \frac{\text{kW}}{\text{m}^2\text{K}} \tag{4}$$

$$h_r = \frac{4.21 \times 10^{-4}}{(1/\varepsilon_g + 1/\varepsilon_w - 1)} \frac{(T_g/100)^4 - (T_w/100)^4}{(T_g - T_w)}, \quad \text{unit} = \frac{\text{kW}}{\text{m}^2\text{K}} \tag{5}$$

where $a$ is a curve fitted constant, which can be obtained from the experimental data; $C_m$ is the mean piston speed (m/s); $\varepsilon_g$ is gas emissivity and $\varepsilon_w$ is wall emissivities.

Eichelberg's model has been widely used to study the heat transfer in large-scale two-stroke and four-stroke diesel engines [11] and can be expressed as

$$h = a \cdot (C_m)^{1/3} \cdot (P_{cyl} \cdot T_g)^{1/2}, \quad \text{unit} = \frac{\text{kW}}{\text{m}^2\text{K}} \tag{6}$$

Annand proposed a heat transfer model based on the steady-state turbulent convection [9,15], as follows:

$$h = a \cdot \frac{k}{B} \cdot Re^{0.7} + b \cdot \frac{(T_g^4 - T_w^4)}{(T_g - T_w)}, \quad \text{unit} = \frac{\text{kW}}{\text{m}^2\text{K}} \tag{7}$$

where $k$ is the thermal conductivity of the fluid; $B$ is the diameter of the engine bore; and $a$ is a curve fitted constant ranging from 0.35 to 0.8 depending on the intensity of charge motion. The constant $b$ is suggested to be $4.3 \times 10^{-12}$ for SI engines. $Re$ is the Reynolds number, which can be expressed as

$$Re = \frac{\rho \cdot C_m \cdot B}{\mu} \tag{8}$$

where $\rho$ is the gas density and $\mu$is the dynamic gas viscosity.

Sitkei's model is used to study the heat transfer in four-stroke indirect injection diesel engines and can be expressed as [15]

$$h = a \cdot (1 + b) \frac{P_{cyl}^{0.7} \cdot C_m^{0.7}}{T_g^{0.2} \cdot (4V_{cyl}/A)^{0.3}}, \quad \text{unit} = \frac{\text{kW}}{\text{m}^2\text{K}} \tag{9}$$

where $V_{cyl}$ is the cylinder volume. The dimensionless constant $b$, which ranges from 0 to 0.35 depending on the type of combustion chamber [7], is used for additional turbulent velocity.

Hohenberg studied the heat transfer for six engines type and proposed a model [10], as follows:

$$h = a \cdot V_{cyl}^{-0.06} \cdot P_{cyl}^{0.8} \cdot T_g^{-0.4} \cdot (C_m + 1.4)^{0.8}, \quad \text{unit} = \frac{\text{kW}}{\text{m}^2\text{K}} \tag{10}$$

where $P_{cyl}$ has the unit of bar.

### 2.2. Proposed model

In order to provide a simple heat transfer model, but yet accurate enough, for the engine simulation, a heat transfer coefficient using the Stanton number $St$ is proposed in this paper, as follows:

$$h = St \cdot \rho \cdot c_p \cdot u \tag{11}$$

where $u$ is the gas turbulent fluctuating velocity, which can be approximated as $0.5C_m$ under the assumption of open combustion chamber without swirl [12]. The factor $c_p$ is the specific heat at constant pressure, and can be expressed as

$$c_p = \frac{R}{1 - (1/\gamma)} \tag{12}$$

where $\gamma$ is the specific heat ratio, which can be obtained using the following equation [20]:

$$\gamma = 1.338 - 6 \times 10^{-5} T_g + 10^{-8} T_g^2 \tag{13}$$

Since $T_w$ is measured on the inside wall surface of the combustion chamber, it might change for different measured locations. In order to eliminate the location dependency, the spark plug temperature $T_c$ is used to replace $T_w$ for the proposed model in this paper.

The most heat energy is generated near the top-dead-center (TDC) and is transferred to the cylinder head surface and piston surface simultaneously. Woschni [18] and Yoo [19] studied the local heat transfer of the piston and cylinder head, and found that about 55% of the heat energy is transferred to the piston and about 45% of that is transferred to the cylinder head. Based on the results in [18,19], the area of heat transfer surface is defined as two times the piston area, i.e. $2A_p$, for obtaining global heat transfer rate.

## 3. Heat flux analysis

### 3.1. Experimental setup

A 125 $\text{cm}^3$ four-stroke air-cooled spark-ignition engine with a single cylinder was employed for developing the heat transfer coefficient in this paper, with specifications as shown in Table 1. Five thermocouples were used to measure the temperatures of the cylinder head at specific positions, as shown in Fig. 1. Two E-type coaxial thermocouples (Medtherm TCS-102-E), $th_1$ and $th_2$, were used to measure the instantaneous temperatures of the inside surface of the cylinder wall near the exhaust and intake valves, respectively. Two K-type thermocouples with Omega 650 temperature indicator, $th_3$ and $th_4$, were used to measure the steady-state temperatures of the outside surface of the cylinder wall near the exhaust and intake valves, respectively. Another K-type thermocouple, $th_{sp}$, was used to measure the temperature of the spark plug $T_{sp}$. The mean cylinder gas temperature $T_g$ was estimated using the state equation of ideal gas as shown in Eq. (2) with the cylinder

Table 1
Specifications of the target engine

| | |
|---|---|
| Engine model | Suzuki AN125 |
| Engine type | Four-stroke, air cooled, OHC |
| Bore × stroke | 52 × 58.6 mm |
| Fuel system | Carburetor |
| No. of valves | 2 |
| Displacement volume | 125 cm$^3$ |
| Compression ratio | 10.2 |
| Idle speed | 1800 rpm |
| Ignition Type | CDI |
| Spark advance | 5°/1500 rpm, 26°/4500 rpm |
| Cylinder head material | Aluminum alloy |
| Combustion chamber | Hemisphere-shaped |

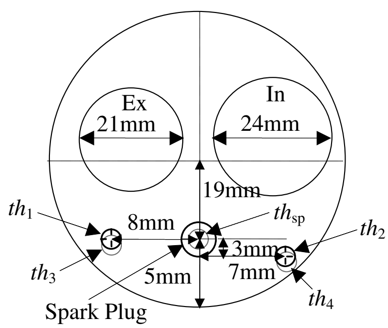


Fig. 1. Inside view of the locations of thermocouples on the cylinder head.

pressure, which was measured with the spark-plug type pressure transducer (Kistler 6117A37).

In order to obtain the engine heat transfer rate for a wide-range of operating conditions, the engine speed was adjusted from 3000 to 6000 rpm at increments of 1000 rpm, and the brake mean effective pressure (BMEP) used as the engine load was adjusted from 1 to 7 bar with an increment of 1 bar.

### 3.2. Heat flux calculation

In most heat flux calculation, the heat flux through the cylinder head wall is assumed to be one-dimensional unsteady heat conduction [1,4,7,9,15]. Since the unsteady heat conduction of the in-wall temperature field exists only within a very small distance from the wall surface, the unsteady component of the temperature gradient perpendicular to the surface is usually much larger than that parallel to the surface. Therefore, one-dimensionality is safely assumed for the unsteady component of the surface heat flux calculation [15]. The heat flux at the combustion chamber can be obtained by solving the following partial differential equation with two boundary conditions.

$$\frac{\partial T}{\partial t} = \alpha \frac{\partial^2 T}{\partial^2 x} \tag{14}$$

where $T$ is the temperature of the cylinder wall, which is a function of $t$ and $x$; $t$ is the time; $x$ is the distance from the

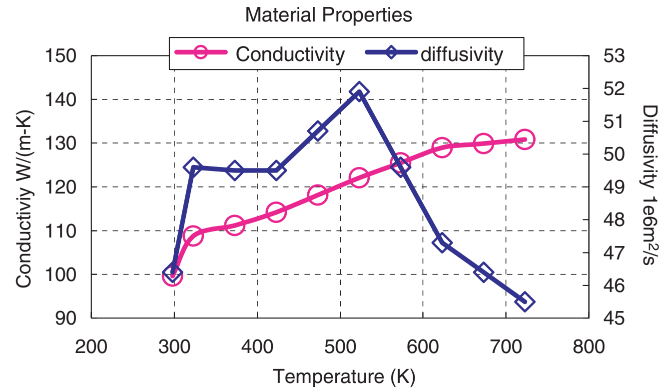


Fig. 2. Material thermal properties [21].

wall surface; $\alpha = k/\rho c$ is the thermal diffusivity; $k$ is the thermal conductivity; and $c$ is the specific heat. The boundary conditions are defined as follows:

$$\begin{aligned} &T(0,t) = T_{\mathrm{wi}}(t) \quad \text{at } x = 0 \\ &T(\ell,t) = T_{\mathrm{wo}}(t) = \text{constant} \quad \text{at } x = \ell \end{aligned} \tag{15}$$

where $T_{\mathrm{wi}}$ is the instantaneous temperature of the cylinder inside wall surface and $T_{\mathrm{wo}}$ is the steady-state temperature of the cylinder outside wall surface with a distance $\ell$ from the inside wall surface. The material properties of the cylinder head with $k$ and $\alpha$ are functions of temperature [21], as shown in Fig. 2.

First, $T_{\mathrm{wi}}$ is represented by the following Fourier series [14]:

$$T_{\mathrm{wi}} = T_{\mathrm{wm}} + \sum_{n=1}^{N} [A_n \cos(n\omega t) + B_n \sin(n\omega t)] \tag{16}$$

where $T_{\mathrm{wm}}$ is the time-averaged value of $T_{\mathrm{wi}}$; $\omega$ is the angular frequency of temperature variation, which is one half of the engine angular velocity for the four stroke engine; and $N$ is the harmonic number which is set to be 200 in this paper.

The solution of Eq. (14) can be expressed as

$$T(x,t) = T_{\mathrm{wm}} - (T_{\mathrm{wm}} - T_{\mathrm{wo}}) + \sum_{n=1}^{\infty} \mathrm{e}^{-c_n x} F_n(x,t) \tag{17}$$

where

$$F_n = A_n \cos(n\omega t - c_n x) + B_n \sin(n\omega t - c_n x) \tag{18}$$

$$A_n = \frac{2}{\tau} \int_0^{\tau} T_{\mathrm{w}}(t) \cos(\omega n t)\, \mathrm{d}t \tag{19}$$

$$B_n = \frac{2}{\tau} \int_0^{\tau} T_{\mathrm{w}}(t) \sin(\omega n t)\, \mathrm{d}t \tag{20}$$

$$c_n = \sqrt{\frac{n\omega}{2\alpha}} \tag{21}$$

The instantaneous heat flux at the cylinder inside wall surface, i.e. $x = 0$, can then be obtained using Fourier's law, as follows:

$$q_w(t) = -k\left(\frac{\partial T}{\partial x}\right)_{x=0}$$
$$= \frac{k}{\ell}(T_{wm} - T_{wo}) + k\sum_{n=1}^{N} c_n[(A_n + B_n)\cos(n\omega t)$$
$$+ (B_n - A_n)\sin(n\omega t)] \quad (22)$$

Since the major heat flux is produced within compression and expansion strokes, $q_w$ is calculated only for these two strokes. The measured temperatures of the cylinder inside wall surface at 6000 rpm with 7 bar BMEP are shown in Fig. 3. As can be seen from Fig. 3, the temperature near the exhaust valve $T_{wi,ex}$ is higher than that near the intake valve $T_{wi,in}$, because the exhaust valve region is heated by the high-temperature exhaust. Both $T_{wi,ex}$ and $T_{wi,in}$ have large temperature gradients near TDC due to the combustion. The corresponding instantaneous heat fluxes $q_{w,ex}$ and $q_{w,in}$ can then be calculated for the exhaust and intake valve regions, respectively, as shown in Fig. 4. The greater the temperature gradient, the higher the heat flux is.

Two instantaneous heat fluxes at the exhaust and intake valve regions are used to represent the average instantaneous heat flux $q_m$, i.e. $q_m = (q_{w,in} + q_{w,ex})/2$. Fig. 5 shows the experimental results with different load conditions at 6000 rpm. The instantaneous heat flux grows with increasing engine loads, because the gas heat transfer coefficient is increased with higher gas pressure and temperature [9,22]. Fig. 6 shows the experimental results with different engine speeds at 6 bar BMEP. Since the gas pressure and temperature do not vary significantly with the engine speed under constant load, the gas heat transfer coefficient changes only slightly with different engine speeds, as does the instantaneous heat flux.

### 3.3. Curve fitted heat flux

For the engine simulation, the heat transfer rate can be obtained using Eq. (1). Since the wall temperature,

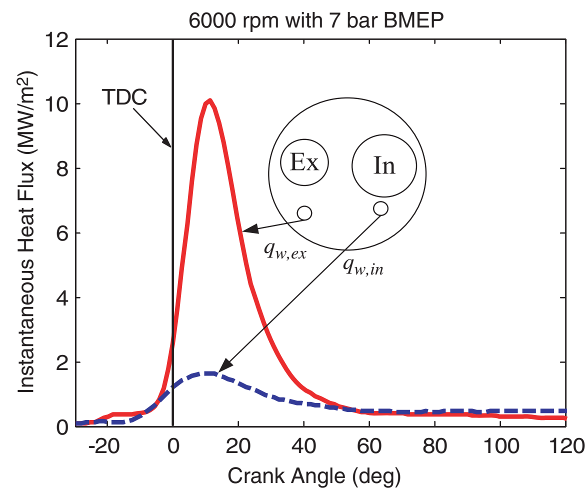


Fig. 4. Instantaneous heat flux variation of the cylinder inside wall surface.

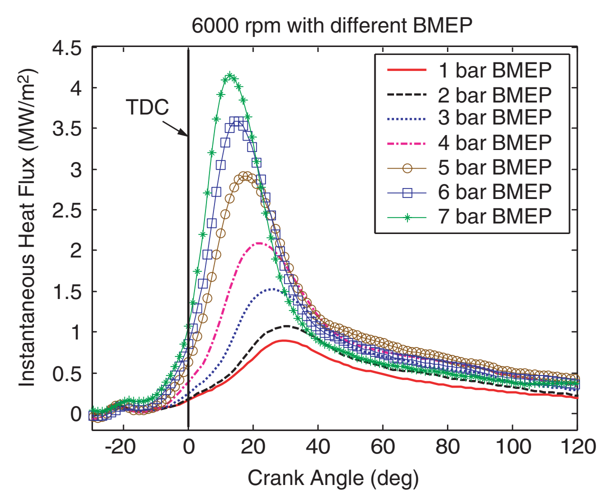


Fig. 5. Heat flux with different engine loads at 6000 rpm.

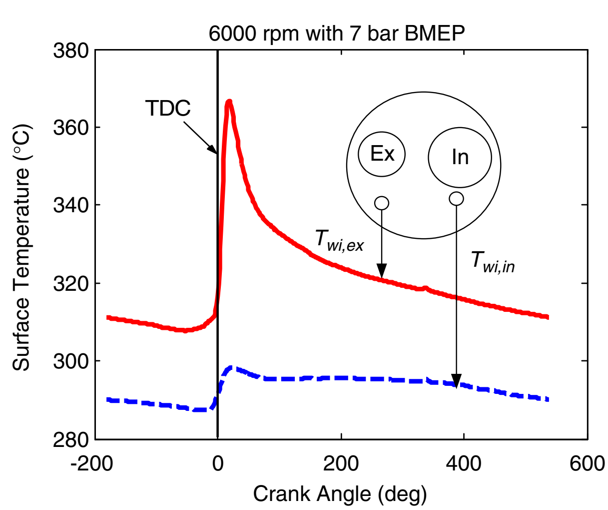


Fig. 3. Temperature variation of the cylinder inside wall surface.

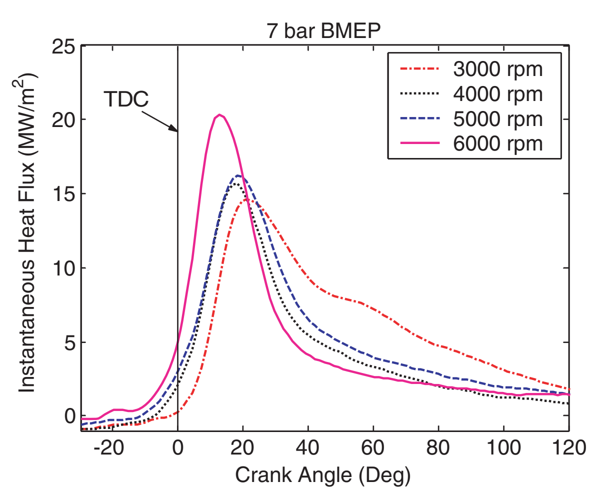


Fig. 6. Heat flux with different engine speeds at 6 bar BMEP.

$T_w$, varies with the crank angle, engine speed, and engine load, it is difficult to simulate the detailed $T_w$. Therefore, $T_w$ is represented as an experimental formula for the compression and expansion strokes in this paper, which can be expressed as

$$T_w = a_{w1} - a_{w2} \cdot \omega_e + a_{w3} \cdot \omega_e^2 - a_{w4} \cdot P_m + a_{w5} \cdot P_m^2 + a_{w6} \cdot \omega_e \cdot P_m, \quad \text{unit} = {}^\circ\text{C} \tag{23}$$

where $\omega_e$ is the engine speed with the unit of rev/second; $P_m$ is the intake manifold pressure with the unit of bar; and $a_{wi}$ is the coefficient obtained from the curve fitting of experimental results and is listed in Appendix 1; the coefficient of determination $R_S$ is used to evaluate correlations between the measured and predicted values of $R_S$ can be expressed as

$$R_S = \frac{\sum_{i=1}^{n}(\hat{y}_i - \bar{y})^2}{\sum_{i=1}^{n}(y_i - \bar{y})^2} \tag{24}$$

where $y$ is the experimental data; $\bar{y}$ is the mean value of experimental data; and $\hat{y}$ is the predicted data. Here, $R_S$ ranges between 0 and 1. If $R_S$ is close to 1, the curve fitted result is close to actual value, and vice versa. The correlation results are shown in Fig. 7. Since $R_S$ is equal to 0.9331, the predicted results are determined to be very close to the experimental data.

In order to compare the predicted heat flux of the previous heat transfer models, the corresponding coefficients $a$ are obtained from the curve fitting of the experimental heat transfer coefficient using the following equation:

$$h = \frac{q_m}{T_g - T_w} \tag{25}$$

where $q_m$ is the averaged experimental instantaneous heat flux during compression and expansion strokes; and $T_g$ and $T_w$ are obtained from Eqs. (2) and (23), respectively. The curve fitted coefficients $a$ of the previous models are shown in Table 2. The $R_S$ of instantaneous heat flux and the heat transfer at cylinder head are used to evaluate the curve fitted results of previous models. The heat transfer at the cylinder head is obtained by integrating the instantaneous heat flux within one cycle using the cylinder head surface as the heat transfer surface. As can been seen from Table 2, of all the previous models, Annand's model gives the best results for both instantaneous heat flux and heat transfer in the cylinder head, and is used to compare with the proposed model in the following section.

Table 2
Curve fitted results of previous models

| | Original $a$ | Fitted $a$ | $R_S$ of the instantaneous heat flux | $R_S$ of the heat transfer at the cylinder head |
|---|---|---|---|---|
| Nusselt | 5.41E-03 | 1.80E-02 | 0.8753 | 0.68051 |
| Eichelberg | 7.67E-03 | 1.20E-02 | 0.9383 | 0.7189 |
| **Annand** | **0.350** | **1.87** | **0.9767** | **0.9401** |
| Sitkei | 2.36E-04 | 1.30E-03 | 0.92375 | 0.77256 |
| Hohenberg | 0.130 | 0.760 | 0.9075 | 0.8507 |

Predicted results of instantaneous heat flux using previous models at 4000 and 6000 rpm with 6 bar BMEP are shown in Figs. 8 and 9, respectively. The predicted results deviated from the experimental value, especially for the high engine speed of 6000 rpm. Although previous models have been curve fitted using the experimental data, they still cannot be widely used for all operating conditions. This might be because the previous models were proposed for large-scale engines, and the heat transfer characteristics of large-scale engines are different from that of small-scale engines.

In order to develop the proposed heat transfer model, the spark plug temperature $T_{sp}$ is used to replace the wall temperature as in Eq. (1). It is represented as an experimental formula, which can be determined from the intake manifold pressure $P_m$ and engine speed $\omega_e$ as

$$T_{sp} = a_{c1} - a_{c2} \cdot \omega_e - a_{c3} \cdot \omega_e^2 - a_{c4} \cdot P_m + a_{c5} \cdot P_m^2 + a_{c6} \cdot \omega_e \cdot P_m, \quad \text{unit} = {}^\circ\text{C} \tag{26}$$

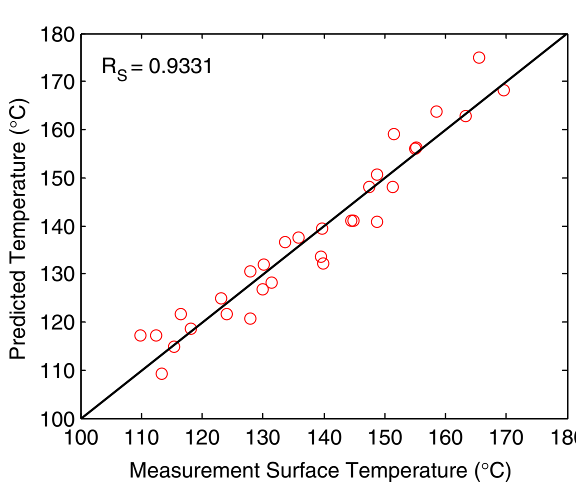


Fig. 7. Correlations between the measured and predicted $T_w$.

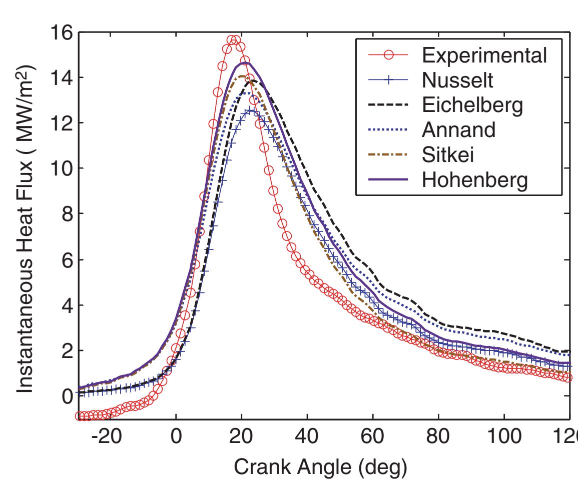


Fig. 8. Predicted heat flux using previous models at 4000 rpm with 6 bar BMEP.

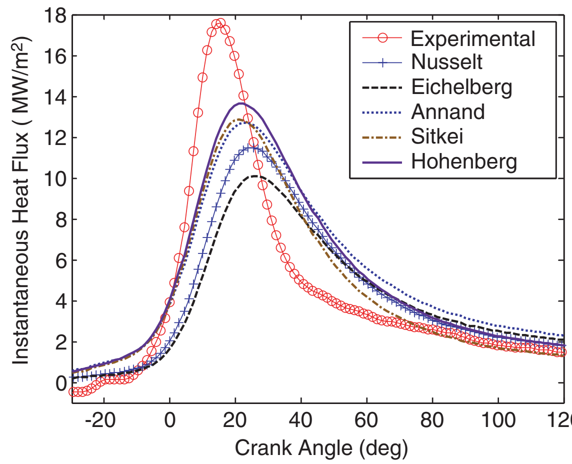


Fig. 9. Predicted heat flux using previous models at 6000 rpm with 6 bar BMEP.

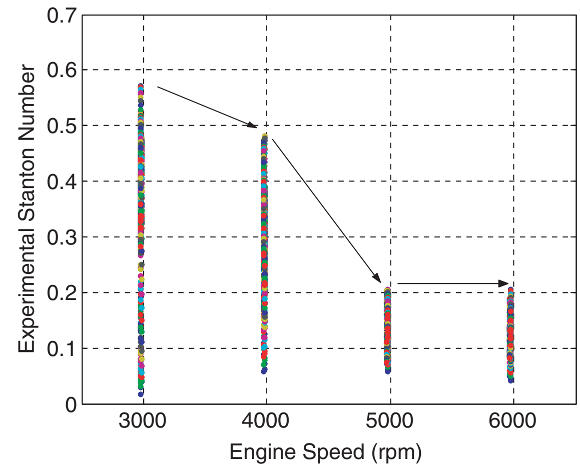


Fig. 11. Correlation of experimental Stanton number and engine speed.

where $a_{ci}$ is the coefficient obtained from the curve fitting of experimental results and is listed in Appendix 1. Correlations between the measured and predicted $T_{sp}$ are shown in Fig. 10. Since $R_S$ is equal to 0.9559, the predicted result is determined to be very close to the experimental data.

In order to develop a heat transfer model for all operating conditions of the target engine, the Stanton number $St$ is employed for the proposed model, as mentioned in Section 2.2. As can be seen from Fig. 11, the Stanton number is varied with engine speed, and presents an exponential tendency. Therefore, this paper employed an exponential function with the engine speed to represent the Stanton number, which is expressed as

$$St = 0.718 \cdot \exp(-0.145 \cdot C_m) \tag{27}$$

Correlations between the predicted and measured instantaneous heat flux are shown in Fig. 12 with $R_S = 0.9980$. Similar results for the heat transfer at the cylinder head are shown in Fig. 13 with $R_S = 0.9979$. Since the $R_S$ of both instantaneous heat flux and heat transfer at the cylinder head are very close to 1, the predicted results of the proposed model are determined to be very close to experimental data.

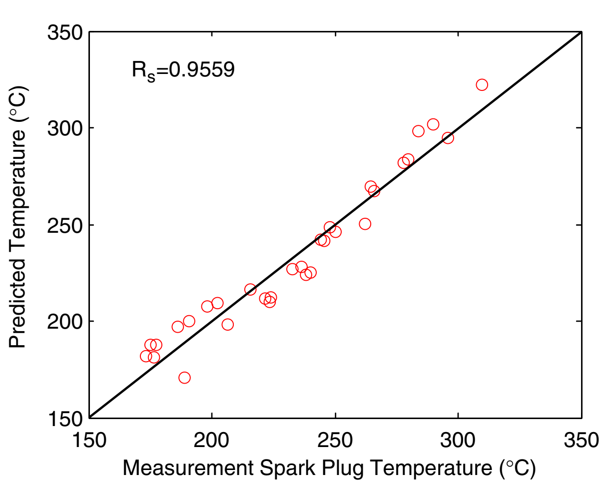


Fig. 10. Correlations between the measured and predicted $T_{sp}$.

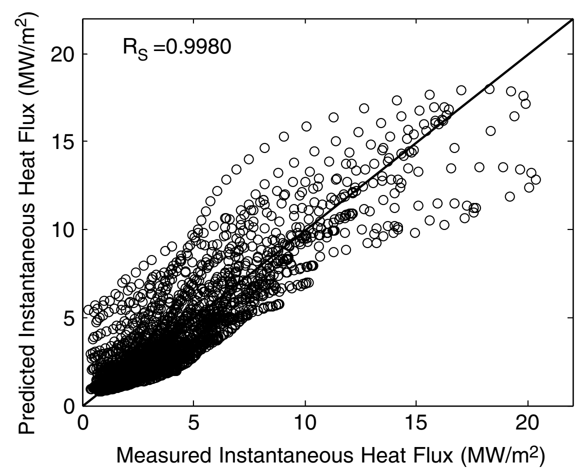


Fig. 12. Correlation between the predicted and measured instantaneous heat flux.

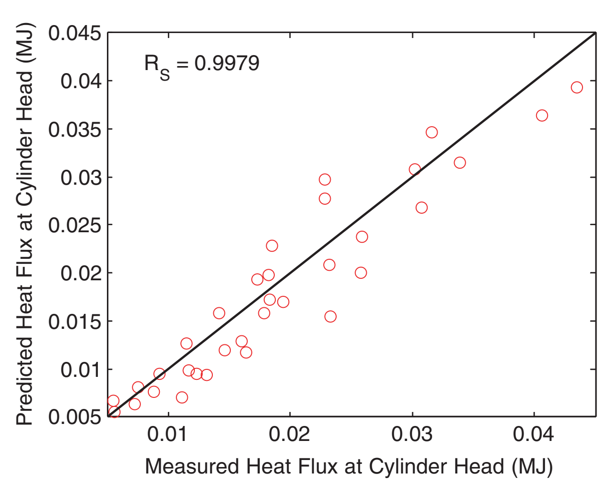


Fig. 13. Correlation between the predicted and measured heat transfer at cylinder head.

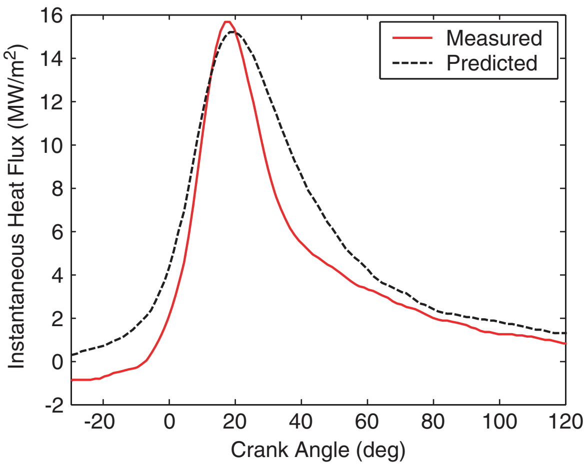


Fig. 14. Predicted and measured instantaneous heat flux at 4000 rpm with 6 bar of BMEP.

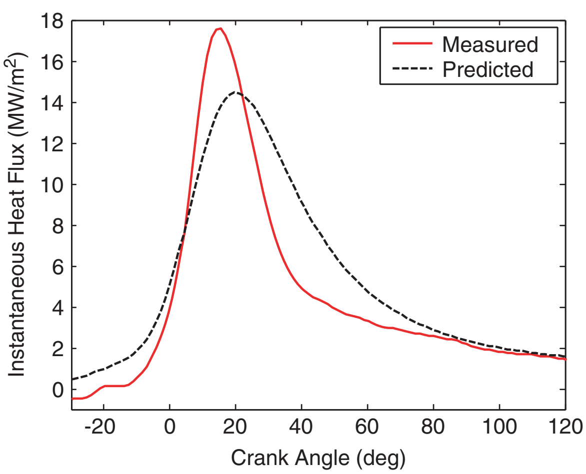


Fig. 15. Predicted and measured instantaneous heat flux at 6000 rpm with 6 bar of BMEP.

Predicted results of instantaneous heat flux using previous models at 4000 and 6000 rpm with 6 bar BMEP are shown in Figs. 14 and 15, respectively. Compared to the previous models, the predicted results of the proposed model are closer to the measured data at different engine speeds.

## 4. Engine model

An engine model is established with Matlab/Simulink as shown in Fig. 16 [23,24]. The charge model is a filling and emptying model based on the one-dimensional isentropic compressible flow equation for predicting the air flow rate. It consists of non-choked and choked flow dynamics as shown in Eqs. (28) and (29), respectively.

$$\dot{m}_{\mathrm{ai}} = \frac{C_{\mathrm{d,im}} A_{\mathrm{th}} P_{\mathrm{atm}}}{\sqrt{R_{\mathrm{a}} T_{\mathrm{atm}}}} \left(\frac{P_{\mathrm{im}}}{P_{\mathrm{atm}}}\right)^{\frac{1}{\gamma_{\mathrm{a}}}} \left\{ \frac{2\gamma_{\mathrm{a}}}{\gamma_{\mathrm{a}} - 1} \left[ 1 - \left(\frac{P_{\mathrm{im}}}{P_{\mathrm{atm}}}\right)^{\frac{\gamma_{\mathrm{a}}-1}{\gamma_{\mathrm{a}}}} \right] \right\}^{\frac{1}{2}},$$

$$\text{when } \frac{P_{\mathrm{im}}}{P_{\mathrm{atm}}} > \left(\frac{2}{\gamma_{\mathrm{a}} + 1}\right)^{\frac{\gamma_{\mathrm{a}}}{\gamma_{\mathrm{a}}-1}} \tag{28}$$

$$\dot{m}_{\mathrm{ai}} = \frac{C_{\mathrm{d,im}} A_{\mathrm{th}} P_{\mathrm{atm}}}{\sqrt{R_{\mathrm{a}} T_{\mathrm{atm}}}} \sqrt{\gamma_{\mathrm{a}}} \left(\frac{2}{\gamma_{\mathrm{a}} + 1}\right)^{\frac{\gamma_{\mathrm{a}}+1}{2(\gamma_{\mathrm{a}}-1)}},$$

$$\text{when } \frac{P_{\mathrm{im}}}{P_{\mathrm{atm}}} \leqslant \left(\frac{2}{\gamma_{\mathrm{a}} + 1}\right)^{\frac{\gamma_{\mathrm{a}}}{\gamma_{\mathrm{a}}-1}} \tag{29}$$

where $\dot{m}_{\mathrm{ai}}$ is the mass airflow through the throttle body; $C_{\mathrm{d,im}}$ is the discharge coefficient of the intake manifold; $A_{\mathrm{th}}$ is the cross-sectional area of the throttle body; $R_{\mathrm{a}}$ is the ideal gas constant of air; $\gamma_{\mathrm{a}}$ is the specific heat ratio of air; $T_{\mathrm{atm}}$ and $P_{\mathrm{atm}}$ are the temperature and pressure of the atmosphere, respectively. The intake manifold pressure $P_{\mathrm{im}}$ is obtained from the state equation of the ideal gas.

$$\frac{\mathrm{d}P_{\mathrm{im}}}{\mathrm{d}t} = \frac{R_{\mathrm{air}} T_{\mathrm{im}}}{V_{\mathrm{im}}} (\dot{m}_{\mathrm{ai}} - \dot{m}_{\mathrm{ao}}) \tag{30}$$

where $V_{\mathrm{im}}$ is the volume of the intake manifold. $\dot{m}_{\mathrm{ao}}$ is the mass airflow from the intake manifold into the cylinder, which can be expressed as

$$\dot{m}_{\mathrm{ao}} = \frac{P_{\mathrm{im}} V_{\mathrm{d}}}{R_{\mathrm{air}} T_{\mathrm{im}} \pi} \omega \eta_{\mathrm{v}} \tag{31}$$

where $V_{\mathrm{d}}$ is the displaced cylinder volume; $\omega$ is the engine speed; and $\eta_{\mathrm{v}}$ is the volumetric efficiency.

The combustion model can be represented using the heat release model, which is a zero-dimensional model based on the first law of thermodynamics [23,24].

$$\frac{\mathrm{d}P_{\mathrm{cyl}}}{\mathrm{d}\theta} = \frac{\gamma_{\mathrm{g}} - 1}{V_{\mathrm{cyl}}} \left( \frac{\mathrm{d}Q_{\mathrm{hr}}}{\mathrm{d}\theta} - \frac{\mathrm{d}Q_{\mathrm{ht}}}{\mathrm{d}\theta} \right) - \frac{\gamma_{\mathrm{g}} P_{\mathrm{cyl}}}{V_{\mathrm{cyl}}} \frac{\mathrm{d}V_{\mathrm{cyl}}}{\mathrm{d}\theta} \tag{32}$$

where $\gamma_{\mathrm{g}}$ is the specific heat ratio of cylinder gas; $P_{\mathrm{cyl}}$ and $V_{\mathrm{cyl}}$ are the pressure and volume of the cylinder, respectively; and $\theta$ is the crank angle. The heat transfer rate is calculated from Eqs. (1), (11) and (27). The heat release rate with respect to the crank angle can be obtained from the rate of mass fraction burned as

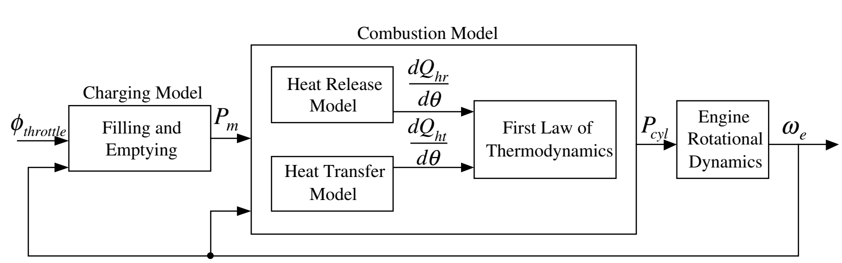


Fig. 16. Block diagram of the engine model.

$$\frac{dQ_{hr}}{d\theta} = a_1 \frac{a_2+1}{\theta_d}\left(\frac{\theta-\theta_0}{\theta_d}\right)^{a_2} \exp\left[-a_1\left(\frac{\theta-\theta_0}{\theta_d}\right)^{a_2+1}\right] Q_{HV} m_f \tag{33}$$

where $m_f$ is fuel mass injected into the cylinder; $\theta_d$ is the total combustion duration expressed in crank angle; $\theta_0$ is the start of combustion; $Q_{HV}$ is the heating value of fuel; $a_1$ and $a_2$ are 5 and 2, respectively [7].

## 5. Verification results

Experimental data of cylinder pressure is used to verify the proposed model. Since Annand's model has the best curve fitting results of the previous models, as shown in Table 2, it is selected for comparison with the model proposed in this paper. In addition, we also investigate whether the heat transfer surface should be used with the proposed $2A_p$ or the entire surface of the combustion chamber.

The comparison of cylinder pressures at 3000 and 6000 rpm with 7 bar BMEP (full load) are shown in Figs. 17 and 18, respectively. Both figures show that the proposed model with $2A_p$ has the predicted results closest to the experimental data, especially for the low speed condition. However, if the heat transfer surface is defined as the entire surface of the combustion chamber, which is shown as Acc in Figs. 17 and 18, it results in underestimated cylinder pressure due to overestimated heat transfer rate.

The comparison of averaged $R_S$ for the proposed model and Annand's model at all engine operating conditions with different areas of the heat transfer surface is shown in Table 3. It is found that the proposed model with $2A_p$ has the largest $R_S$, i.e. the best prediction results.

In order to compare the proposed model and Annand's model with $2A_p$ at all engine operating conditions, the difference between the $R_S$ of the proposed model $R_{S,Proposed}$ and the $R_S$ of the Annand's model $R_{S,Annand}$ is defined as

$$\Delta R_S = R_{S,Proposed} - R_{S,Annand} \tag{34}$$

If $\Delta R_S$ is positive, the proposed model performs better than Annand's model, and vice versa. The results of $\Delta R_S$ at all operating conditions are shown in Table 4. As can been seen from Table 4, the proposed model has closer prediction results than Annand's model at most engine operation conditions with a positive mean value of 0.105, which is about twice the magnitude of the negative mean value of −0.018 at the other engine operating conditions.

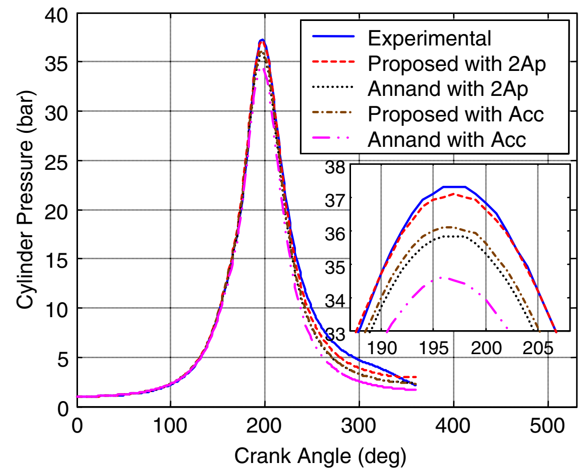


Fig. 18. Comparison of the cylinder pressure at 6000 rpm with 7 bar BMEP (full load).

Table 3
Averaged $R_S$ of the cylinder pressure at all engine operating conditions

| | Proposed with $2A_p$ | Annand with $2A_p$ | Proposed with Acc | Annand with Acc |
|---|---|---|---|---|
| Averaged $R_S$ | 0.949 | 0.862 | 0.851 | 0.829 |

Table 4
$\Delta R_S$ of the cylinder pressure

| $\omega_e$ (rpm) | BMEP | | | | | | |
|---|---|---|---|---|---|---|---|
| | 1 bar | 2 bar | 3 bar | 4 bar | 5 bar | 6 bar | 7 bar |
| 3000 | −0.046 | **0.023** | **0.049** | **0.084** | **0.095** | **0.090** | **0.042** |
| 4000 | −0.008 | **0.197** | **0.140** | **0.016** | −0.006 | **0.017** | **0.034** |
| 5000 | **0.167** | **0.221** | **0.155** | **0.076** | **0.065** | −0.014 | **0.021** |
| 6000 | **0.162** | **0.245** | **0.303** | **0.107** | **0.074** | **0.021** | **0.106** |

*Note*: negative mean value = −0.018; positive mean value = 0.105.

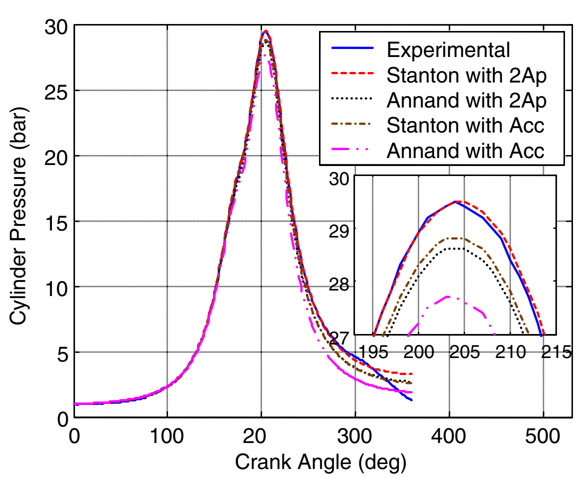


Fig. 17. Comparison of the cylinder pressure at 3000 rpm with 7 bar BMEP (full load).

## 6. Conclusions

The heat transfer models proposed by Nusselt, Eichelberg, Annand, Sitkei, and Hohenberg are not suitable for small-scale SI engines because they were developed primarily for diesel engines and large-scale SI engines. After curve fitting of the experimental data of a 125 $cm^3$ air-cooled SI engine, Annand's model has the closest prediction results of the previous models. However, it still cannot be widely used for all operation conditions, perhaps because the previous models were proposed for large-scale engines, and the heat transfer characteristics of large-scale engines are different from that of the small-scale ones. In order to develop a heat transfer model suitable for small-scale SI engines, a model using the Stanton number, which is much simpler but yet accurate enough, is proposed in this paper. The area of heat transfer surface is defined as two times the piston area, i.e. $2A_p$, for the proposed model. Experimental data for cylinder pressure were used to verify the proposed model. The results show that the proposed model has better prediction results than the Annand's model at most engine operation conditions. It was also found that the prediction results of the cylinder pressure using $2A_p$ as the heat transfer surface is more accurate than that using the entire surface of the combustion chamber.

## Acknowledgement

The authors would like to thank the Industrial Technology Research Institute (ITRI, Taiwan) for providing the experimental data and the National Science Council (NSC, Taiwan) for financial support (NSC-93-2212-E-027-009).

## Appendix 1

See Table A.1.

Table A.1
Coefficients of $T_c$ and $T_w$

| | | | |
|---|---|---|---|
| $a_{w1}$ | 1408.7 | $a_{c1}$ | 1176.2 |
| $a_{w2}$ | 9.3021 | $a_{c2}$ | 2.4074 |
| $a_{w3}$ | $4.7205 \times 10^{-3}$ | $a_{c3}$ | 0.017601 |
| $a_{w4}$ | 2640.1 | $a_{c4}$ | 2603.8 |
| $a_{w5}$ | 1423.4 | $a_{c5}$ | 1540.4 |
| $a_{w6}$ | 9.8922 | $a_{c6}$ | 6.3406 |

## Appendix 2

See Tables A.2–A.5.

Table A.2
$R_S$ of the proposed model with $2A_p$

| $\omega_e$ (rpm) | BMEP | | | | | | |
|---|---|---|---|---|---|---|---|
| | 1 bar | 2 bar | 3 bar | 4 bar | 5 bar | 6 bar | 7 bar |
| 3000 | 0.895 | 0.851 | 0.962 | 0.942 | 0.903 | 0.876 | 0.971 |
| 4000 | 0.772 | 0.960 | 0.986 | 0.988 | 0.994 | 0.999 | 0.995 |
| 5000 | 0.929 | 0.932 | 0.928 | 0.973 | 0.984 | 0.974 | 0.998 |
| 6000 | 0.942 | 0.936 | 0.989 | 0.954 | 0.971 | 0.973 | 0.992 |

Mean = 0.949.

Table A.3
$R_S$ of the Annand's model with $2A_p$

| $\omega_e$ (rpm) | BMEP | | | | | | |
|---|---|---|---|---|---|---|---|
| | 1 bar | 2 bar | 3 bar | 4 bar | 5 bar | 6 bar | 7 bar |
| 3000 | 0.941 | 0.828 | 0.912 | 0.858 | 0.808 | 0.787 | 0.929 |
| 4000 | 0.780 | 0.763 | 0.846 | 0.971 | 0.999 | 0.982 | 0.961 |
| 5000 | 0.762 | 0.711 | 0.773 | 0.897 | 0.919 | 0.988 | 0.976 |
| 6000 | 0.780 | 0.691 | 0.686 | 0.847 | 0.898 | 0.952 | 0.886 |

Mean = 0.862.

Table A.4
$R_S$ of the proposed model with the entire surface of the combustion chamber

| $\omega_e$ (rpm) | BMEP | | | | | | |
|---|---|---|---|---|---|---|---|
| | 1 bar | 2 bar | 3 bar | 4 bar | 5 bar | 6 bar | 7 bar |
| 3000 | 0.768 | 0.850 | 0.826 | 0.873 | 0.976 | 0.961 | 0.900 |
| 4000 | 0.796 | 0.697 | 0.716 | 0.819 | 0.867 | 0.871 | 0.950 |
| 5000 | 0.746 | 0.728 | 0.787 | 0.854 | 0.879 | 0.956 | 0.960 |
| 6000 | 0.787 | 0.759 | 0.765 | 0.883 | 0.921 | 0.973 | 0.962 |

Mean = 0.851.

Table A.5
$R_S$ of the Annand's model with the entire surface of the combustion chamber

| $\omega_e$ (rpm) | BMEP | | | | | | |
|---|---|---|---|---|---|---|---|
| | 1 bar | 2 bar | 3 bar | 4 bar | 5 bar | 6 bar | 7 bar |
| 3000 | 0.815 | 0.887 | 0.877 | 0.950 | 0.921 | 0.856 | 0.867 |
| 4000 | 0.897 | 0.690 | 0.674 | 0.793 | 0.871 | 0.881 | 0.889 |
| 5000 | 0.797 | 0.673 | 0.692 | 0.763 | 0.816 | 0.909 | 0.932 |
| 6000 | 0.961 | 0.874 | 0.644 | 0.724 | 0.792 | 0.890 | 0.886 |

Mean = 0.829.

## References

[1] T. Oguri, On the coefficient of heat transfer between gases and cylinder walls of the spark-ignition engine, Bull. JSME 3 (11) (1960) 363–369.
[2] A.C. Alkidas, Heat transfer characteristics of a spark-ignition engine, ASME J. Heat Transfer 102 (1980) 189–193.
[3] A.C. Alkidas, J.P. Myers, Transient heat-flux measurements in the combustion chamber of a spark-ignition engine, ASME J. Heat Transfer 104 (1982) 62–67.
[4] A.C. Aldidas, I.-S. Suh, The effects of intake-flow configuration on the heat-release and heat-transfer characteristics of a single-cylinder four-valve SI engine, SAE Paper No. 910296, 1991.
[5] P.J. Shayler, S.A. May, T. Ma, The determination of heat transfer from the combustion chambers of SI engines, SAE Paper No. 931131, 1993.
[6] A. Franco, L. Martorano, Evaluations on the heat transfer in the small two-stroke engines, SAE Paper No. 980762, 1998.
[7] J.B. Heywood, Internal Combustion Engine Fundamentals, McGraw-Hill, New York, 1988, pp. 668–711.
[8] C.F. Taylor, Int. Combust. Eng. Theory Practice, 1, MIT Press, Cambridge, MA, 1966, pp. 266–290.
[9] W.J.D. Annand, Heat transfer in the cylinders of reciprocating internal combustion engines, Proceedings of the Institution of Mechanical Engineers 177 (36) (1963) 973–990.
[10] G.F. Hohenberg, Advanced approaches for heat transfer calculations, Diesel Engine Thermal Loading, SAE SP-449, 1979, pp. 61–79.

[11] G. Eichelberg, Some new investigations on old combustion engine problems, Engineering 148 (1939) 463–547.

[12] V.D. Overbye, J.E. Bennethum, O.A. Uyehara, P.A. Myers, Unsteady heat transfer in engines, SAE Trans. 69 (1961) 461–494.

[13] G. Woschni, A universally applicable equation for the instantaneous heat transfer coefficient in the internal combustion engine, SAE Trans. 76 (1967) 3065–3084.

[14] G. Lindfield, J. Penny, Numerical Methods Using Matlab, Prenticae Hall, 1999.

[15] G. Borman, K. Nishiwaki, Internal-combustion engine heat transfer, Prog. Energy Combust. Sci. 13 (1987) 1–46.

[16] W. Nusselt, Die Wärmeübergang in den Verbrennungs-kraftmaschinen, Z. VER. Dtsch. Ing 67 (1923) 692–708.

[17] J.L. Lumley, Engines an Introduction, Cambridge University Press, 1999, pp. 95–117.

[18] G. Woschni, J. Fieger, Determination of local heat transfer coefficients at the piston of a high speed diesel engine by evaluation of measured temperature distribution, SAE Paper No. 790834, 1979.

[19] S.-J. Yoo, E.-S. Kim, A study of in-cylinder local heat transfer characteristic of a spark ignition engine, SAE Paper No. 931981, 1993.

[20] M.F.J. Brunt, H. Rai, L.A. Emtage, The calculation of heat release energy from engine cylinder pressure data, SAE Paper No. 981052, 1998.

[21] P. Labelle, M. Pekgularyuz, R. Bouchard, New aspects of temperature behavior of AJ52x, Creep Resistant Magnesium Alloy, SAE Paper No. 2002-01-0079, 2002.

[22] C.D. Rakopoulos, G.C. Mavropoulos, D.T. Hountalas, Measurements and analysis of load and speed effects on the instantaneous wall heat fluxes in a direct injection air-cooled diesel engine, Int. J. Energ. Res. 24 (7) (2000) 587–604.

[23] Y.-Y. Wu, Y. Shiao, B.-C. Chen, Motorcycle engine modeling for real time control, in: 6th International Symposium on Advanced Vehicle Control, Hiroshima, Japan, JSAE 20024526, 2002.

[24] B.-C. Chen, Y.-Y. Wu, F.-C. Hsieh, Estimation of engine rotational dynamics using closed-loop estimator with stroke identification for engine management systems, Proceedings of the Institution of Mechanical Engineers. Part D. J. Automobile Eng. 219 (12) (2005) 1391–1406.